J Nanopart Res (2023) 25:138
https://doi.org/10.1007/s11051-023-05781-8

RESEARCH PAPER

Study of CO molecules on $Pd/Al_2O_3/NiAl(110)$ surface by atomic force microscopy and Kelvin probe force microscopy

Shanrong Zou · Jiuyan Wei · Qiang Zhu · Hongqian Sang · Yasuhiro Sugawara · Yan Jun Li

Received: 25 January 2023 / Accepted: 5 June 2023 / Published online: 30 June 2023

Abstract Reactant adsorption sites of novel metal catalysts are difficult to characterize precisely, which is vital for understanding heterogeneous reactions and designing efficient catalytic systems. However, even at cryogenic temperatures, a complete atomic understanding of catalytic reaction sites remains elusive, such as the variation in reactant molecule adsorption sites on metal nanoclusters (NCs). Here, we studied CO adsorption on the Pd NC of an $Al_2O_3/NiAl(110)$ surface with atomic resolution by noncontact atomic force microscopy and Kelvin probe force microscopy at room temperature. We found that CO molecules are preferentially adsorbed on the Pd NC (~2 nm) on line defects. We investigated the consecutive scanning topographic AFM images of CO molecules on the $Pd/Al_2O_3/NiAl$ surface and found the most stable adsorption site of CO molecules on bridge site and the most unstable adsorbed site on step_110, which are supported by density functional theory (DFT) calculations. This result reveals that the electronic and geometric properties of Pd NCs and CO molecules are expected to provide insight into the mechanism of Pd-based heterogeneous catalysis.

Keywords Palladium nanoparticle · CO adsorption sites · Heterogeneous catalysis · $Al_2O_3/NiAl(110)$ surface · Nanostructured catalysts

S. Zou · J. Wei · Q. Zhu · Y. Sugawara · Y. J. Li (✉)
Department of Applied Physics, Graduate School of Engineering, Osaka University, 2-1 Yamadaoka, Suita, Osaka 565-0871, Japan
e-mail: liyanjun@ap.eng.osaka-u.ac.jp

H. Sang
Institute for Interdisciplinary Research, Jianghan University, Sanjiaohu Rd, Caidian District, Wuhan 430014, Hubei, China

Introduction

In heterogeneous catalysis, reactants adsorb onto the surface of the catalyst, and the availability of reaction active sites can limit the rate of heterogeneous reaction [1–4]. Heterogeneous catalysts are difficult to characterize precisely, and many studies have been conducted to locate active sites on various catalytic materials. Observations of the adsorption sites of reactants have shown that metal oxide interfaces are catalytically the most active, such as planar Au clusters on MgO/Ag(001) thin films and Pt clusters on graphene/Rh(111) [5, 6]. Furthermore, catalytic activity is related to the local charge state, and the catalytic activity of Au clusters on a MgO substrate can be enhanced by locally charging the substrate [7]. The ratio of neutral to cationic Pt atoms in the Pt nanocluster(NC) was found to be strongly correlated with the CO oxidation activity [8].

Palladium (Pd) catalyzes the conversion of polluting hydrocarbons, carbon monoxide, and nitrogen oxide in automobile exhaust to water, carbon dioxide, and nitrogen in catalytic converters, respectively [9]. Pd nanoparticle (NP) catalysts have high performance for sustainable liquid-phase reactions [10]. Pd NCs are introduced to the catalytic system for catalyzing the CO + O_2 reaction at 300 K [11]. In addition, theoretical calculations have shown that in Pd NCs of ~4 nm diameter, the edge and corner sites have a good activity [12]. However, the atomic resolution of Pd NPs has not been investigated on the Al_2O_3/NiAl(110) surface at room temperature (RT), which is vital for understanding the CO adsorption sites in heterogeneous catalysis.

To date, the adsorption of a single CO molecule on transition metal NPs is characterized by various of averaging techniques. It was demonstrated by infrared multiple photon dissociation (IR-MPD) spectroscopy that the CO molecule only shows the top binding of both nickel and platinum, whereas Pd clusters exhibit various of binding sites [13]. By using the STM technique, the adsorption sites and manipulation processes can be investigated, which enables the individual visualization of CO molecules [14]. Non-contact atomic force microscopy (NC-AFM) has been used to quantify the force performance required to move CO laterally, the interaction between a CO molecule and an adatom or another CO molecule, and the manipulation of its tilting [15–19]. Furthermore, some studies have shown the CO adsorption sites on a metal surface on basis of molecular orbital principles in terms of DFT or on a single Pd-Fe_3O_4 catalyst by STM in real time [20, 21]. More recently, CO-terminated tips have been used to probe chemical binding forces on single Fe atoms to elucidate the individual atoms chemical reactivity within flat Fe clusters depending on the coordination number of the investigated atom [22]. Actually, the CO molecule can be activated at RT with the Pd NC participation, therefore, the spatial visualization CO molecule adsorption sites on the NC is a challenge.

In this work, we performed the NC-AFM and KPFM to investigate the adsorption behavior of CO molecules on a Pd/Al_2O_3/NiAl(110) surface with atomic resolution at RT. We found the preferential adsorption site of CO molecules, which was analyzed by DFT calculation.

Experimental methods

NC-AFM

The experiments were performed using a home-built NC-AFM system under ultrahigh vacuum at RT [23–25]. An Ir-coated Si cantilever (NANOSENDORS) with a resonance frequency of 1.13 MHz was used. The NC-AFM system was used in the frequency-modulation detection method with a constant oscillation amplitude (800 pm) [26–28]. All images were obtained in the constant-frequency mode. Electrostatic force (F_ω) between the AFM tip and sample is given by $F_\omega = -\frac{\partial C(z)}{\partial z}(V_{DC} - V_{CPD})V_{AC}\sin(\omega t)$, where z is the direction normal to the sample surface, V_{CPD} is the potential difference and C is the capacitance between tip and sample surface separately.V_{DC} nullifies the oscillating electrical forces that originated from CPD between tip and sample surface. In our case, the local contact potential difference (LCPD) voltage can be determined with a feedback loop using KPFM.

Sample preparation

The NiAl(110) surface was prepared by cyclic of Ar ion sputtering and annealing at 1000 °C. The alumina thin film was obtained by exposing 1000 L of O_2 to the NiAl(110) surface, followed by annealing at 380-400 °C. Pd was evaporated onto alumina thin film surfaces using an electron beam evaporator (Omicron EFM 3) at RT. The deposition rate of the evaporator was 6.4×10^{17} atoms/cm^2 · s (about 0.13 ML/min) for 2 min. CO molecules (purity 99.9%) were dosed as received via a high precision UHV leakage valve. The CO pressure was controlled using the ion gauges.

DFT calculation details of CO adsorption on Pd/alumina-NiAl (110)

A periodically repeated slab model was used to investigate the CO adsorption on Pd cluster supported alumina-NiAl (110) surface within the generalized gradient approximation using Quantum-ESPRESSO package [29, 30]. The generalized gradient approximation was adopted by the Perdew-Burke-Ernzerhof (PBE) density functional to describe electronic exchange and correlation [31]. The surface

was modeled using an alumina-NiAl (110) [32, 33] with a Pd_{24+13} cluster (Pd-Pd bond length of 2.75 Å) adsorbed on the surface [34, 35]. The model was calculated for the two layers of alumina which were formed by a parallelogram-shaped supercell with two oxide unit cells placed onto 33 NiAl unit cells. The alumina atomic coordinates were determined by previous theoretical studies combined with AFM/STM results [33, 37, 38]. The position of the 37 Pd atoms on the alumina subtract was determined based on the AFM result after relaxed geometries. The Broyden-Fletcher-Goldfarb-Shanno (BFGS) algorithm has been used for geometry optimizations, with residual forces as 0.01 eV/Å and 5.4×10^{-4} eV energy variation [36, 37]. In the z direction, slabs were separated from their periodic images by a 15 Å vacuum gap. Wave functions were expanded in plane waves with a kinetic energy cutoff of 400 eV.

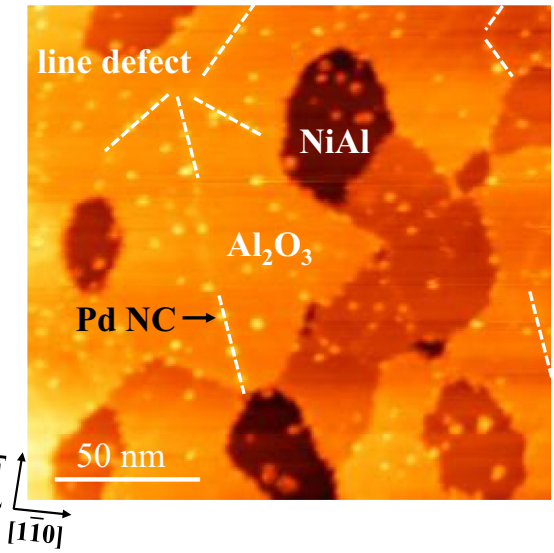

Fig. 1 Topographic AFM image of $Pd/Al_2O_3/NiAl$ surface at room temperature. Bright dot: Pd nanoclusters. Dashed line: line defect. Parameters: constant-Δf mode, $f_0 = 1.12$ MHz, Q = 3304, A = 800 pm, and size: 180×180 nm^2

Results and discussion

Figure 1 shows a large-area NC-AFM image of Pd NCs deposited on an $Al_2O_3/NiAl$ surface, which contains a series of line defects. The line defects are nucleation sites and act as the electron transfer pathway of the $Al_2O_3/NiAl(110)$ surface at RT [33, 38–40]. Here, bright spots indicate Pd nanoclusters, dashed lines indicate line defects and the dark contrast indicates the NiAl substrate; the others are Al_2O_3 domains. Next, we exposed CO molecules and investigated their adsorption behavior in the same area.

Figure 2 shows topographic AFM and CPD images simultaneously on $Pd/Al_2O_3/NiAl$ surface. Figure 2(a) and (b) show topographic AFM images obtained before and after CO adsorption, and Fig. 2(c) and (d) show CPD images corresponding to Fig. 2(a) and (b). After CO molecule adsorption, the size of some Pd NCs on the terrace become small as shown by white arrows in Fig. 2(b) and the corresponding CPD contrasts become dark in Fig. 2(d), whereas the Pd NCs become large on the terrace as shown by black arrow in Fig. 2(b) and the CPD contrast becomes bright in Fig. 2(d). We found that Pd NC has almost no change in size on the line defect compared with that on terrace as shown by dot circle in Fig. 2(b). In Fig. 2(c), before CO molecule adsorption, Pd NCs adsorbed on line defect and terrace show bright contrast in CPD image, which are negatively charged and consistent with the previous results [38, 39]. In Fig. 2(d), after CO molecule adsorption, the Pd NCs show dark contrast, which indicated the positive or neutral charge state. To obtain insight into the adsorption activity after CO exposure to $Pd/Al_2O_3/NiAl$ surface, the enlarger images were taken in Fig. 2(e) and (f). After CO exposure, more CO molecules as dark spots prefer to adsorb on Pd NC on line defect than on terrace as shown in Fig. 2(e). We found that CO molecules adsorbed on top of Pd NC on line defect, whereas CO molecules adsorbed on edge Pd NC on terrace. In addition, CO adsorbed Pd NC on line defect as the bright contrast was obtained in the CPD image whereas dark contrast on the terrace as shown in Fig. 2(f). This result reveals more negatively charged on line defect and more positively charged or neutral charge state on terrace. Note that it is difficult to identify the details of CO preferably adsorption site on Pd NC on line defect in Fig. 2(e). While, it is easy to clarify CO preferably adsorption site on edge of Pd NC on terrace because of more numbers of CO adsorbed on edge than on top of Pd NC. To get the more information of CO molecules on Pd NC, we will investigate the line profiles before and after CO adsorption on Pd NC and measure the force curves in the next.

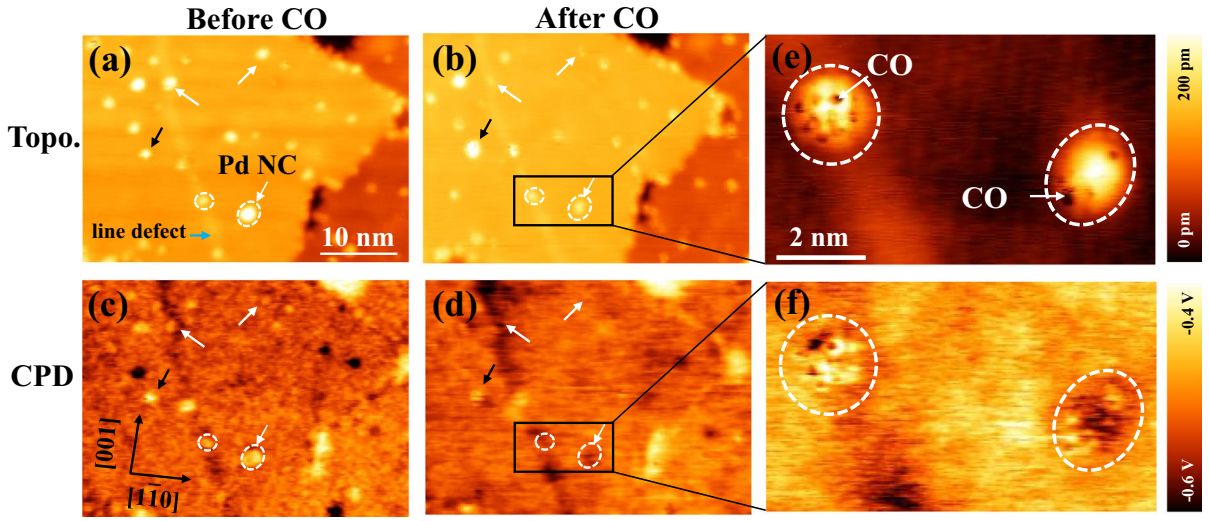

Fig. 2 Topographic AFM and CPD images of $Pd/Al_2O_3/NiAl$ surface. Topographic AFM images obtained **(a)** before and **(b)** after CO adsorption with 30 min under the pressure of 1×10^{-6}torr. CPD images obtained **(c)** before and **(d)** after CO adsorption. **(e)** and **(f)** Enlarger images of rectangles in **(b)** and **(d)**, respectively. White arrows: the Pd NCs become small in **(b)** after CO adsorption. Blue arrow: line defect, black arrow: Pd NCs become large in **(b)** after CO adsorption and dark spots: CO molecules in **(e)**. Parameters: constant-Δf mode, f_0 = 1.12 MHz, Q = 3304, V_{AC} = 500m V, f_{AC} = 190 Hz. Size: 85 × 58 nm^2. Enlarger size: 8.8 × 5 nm^2

Figure 3(a) and (b) show the topographic AFM images of Pd NCs on line defect before and after CO molecules adsorption and corresponding line profiles in Fig. 3(c) and (d). We found that the height of the Pd NCs decreased after the CO adsorption marked by blue arrows in Fig. 3(c). Because the attractive interaction between tip with Pd is stronger than that with CO molecule. The bond length of CO on the Pd NCs is around 60 pm, which is smaller than that in the gas phase [18]. In addition, the force curves on top of the CO molecule and Al_2O_3 surface were shown in Fig. 3(e), the inset indicates the interaction model between the tip and the CO molecule according to the previous theory [41]. The force curve on the CO molecule shows two minima at various tip sample distance compared with surface, which can be assigned to the physisorption and chemisorption minima, as shown by previous results and the theory [19]. Thus, this feature represents the interaction between O-terminated CO and metal atoms, which can be used to distinguish the CO molecule. The force deconvolution method was proposed by Sader [42]. The minimum force is 0.68 nN, which is related to the coordination number of the investigated CO molecule. Next, we will investigate CO adsorption with different CO exposing time.

To clarify CO preferably adsorption site on edge of Pd NC on terrace, we investigated CO adsorption with different CO exposing time. The result is shown in Fig. 4, in which we found that CO gradually adsorbs on edge of Pd NC on the terrace as shown by dot circles. The number of adsorbed CO molecules affects the electronic properties of the Pd NC, which can be interpreted from the CPD image in Fig. 2(f).

To get more information of CO adsorption sites, we performed consecutive scanning topographic AFM images of CO molecules on $Pd/Al_2O_3/NiAl$ surface with recording every 20 min after 90 min of CO adsorption. Figure 5(a) - (e) are the result of topographic images in the constant-frequency mode. The adsorption and desorption of CO molecules on the Pd NC can be found with scanning times. Here, CO molecules are imaged as a depression contrast on different sites of the Pd NC in the AFM images, owing to the repulsive interaction with the tip apex. Figure 5(f) - (j) are schematic models of CO adsorption on two layers of the Pd NC, according to experimental results. Figure 5(k) - (o) show the AFM images with the models which match each other well. A control experiment without CO exposure was done which showed no change in the Pd NC structure within

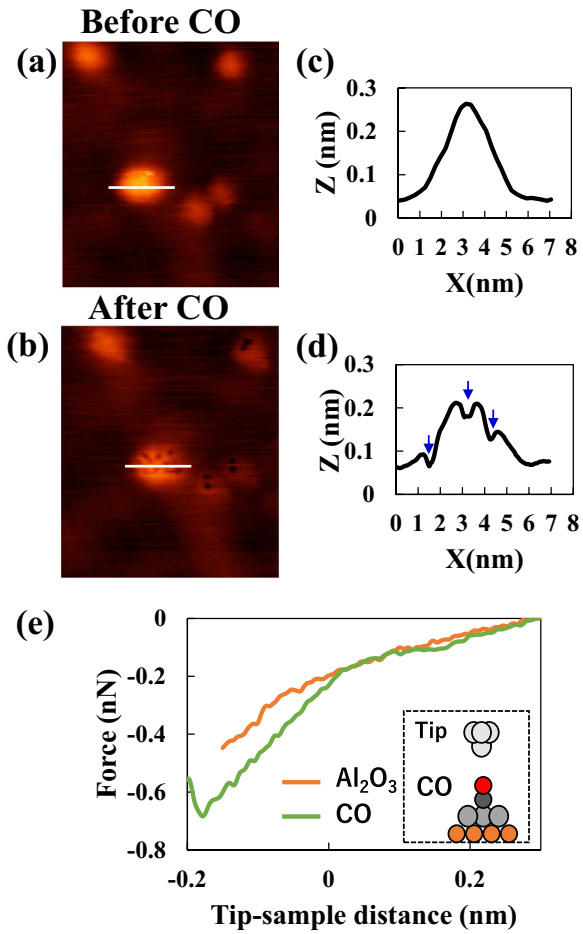

Fig. 3 Topographic AFM images obtained before **(a)** and after **(b)** CO adsorption on $Pd/Al_2O_3/NiAl$ surface. **(c)** and **(d)** Line profiles corresponding to **(a)** and **(b)**, respectively. **(e)** Force curves on sites of CO and Al_2O_3

90 mins. Furthermore, we calculate and assign the adsorption sites of the CO molecule as shown below.

The CO adsorption model of the Pd NC on the Al_2O_3 surface was proposed on the basis of DFT calculations in Fig. 6. Figure 6(a) is the top view of two layers of Pd NCs adsorbed on the Al_2O_3 surface. Figure 6(b) - (e) are the side views of the CO molecule adsorbed on the top site, bridge site, step_111 site, and step_110 site on the Pd NC, respectively, and the carbon atom attaches to the Pd atom to form O termination [27, 28]. In the calculation model, the O atoms and C atoms of CO molecules are indicated in red and brown balls, the first and second-layer Pd atoms are indicated by grey and yellow balls, and the Al and O atoms of Al_2O_3 the surface are indicated by green and black balls, respectively. We concluded that the adsorption of CO molecules is distributed on the top, bridge, step_110, and step_111 sites of the Pd NC. This consistent with the experimental results shown in Fig. 5

Theoretical studies of CO molecule adsorption sites on alumina supported Pd cluster were proposed. The CO adsorption energies (E_a) are computed from the difference of total energies of the Pd/alumina slab + CO adsorbate system and the noninteracting clean Pd/alumina slab and gas-phase CO molecule in Eq. 1. As shown in Table 1, the adsorption energy at the top, bridge, step_111 and step_110 are -2.95, -3.68, -1.66 and -1.07 eV, respectively. This result indicates that the most stable adsorption site of CO molecule is the bridge site, followed by the top site. And the most unstable adsorbed site was step_110. Our experiment results matched DFT calculations and eventually dissociates from step_110 and finally forms a stable structure adsorbed at the bridge site.

$$E_a = E_{CO/Pd/Al_2O_3} - E_{CO} - E_{Pd/Al_2O_3}$$

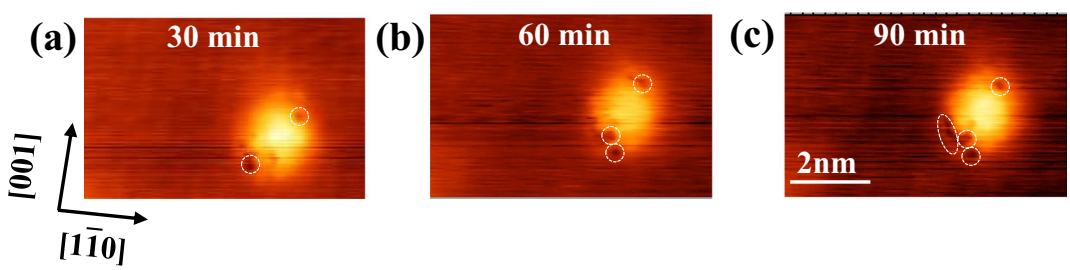

Fig. 4 Topographic AFM images after CO adsorption on $Pd/Al_2O_3/NiAl$ surface with different CO exposing time. **a** 30 min of CO adsorption (1×10^{-6}torr), **b** 60 min, **c** 90 min. The CO molecules marked by dot circles increase with adsorption time

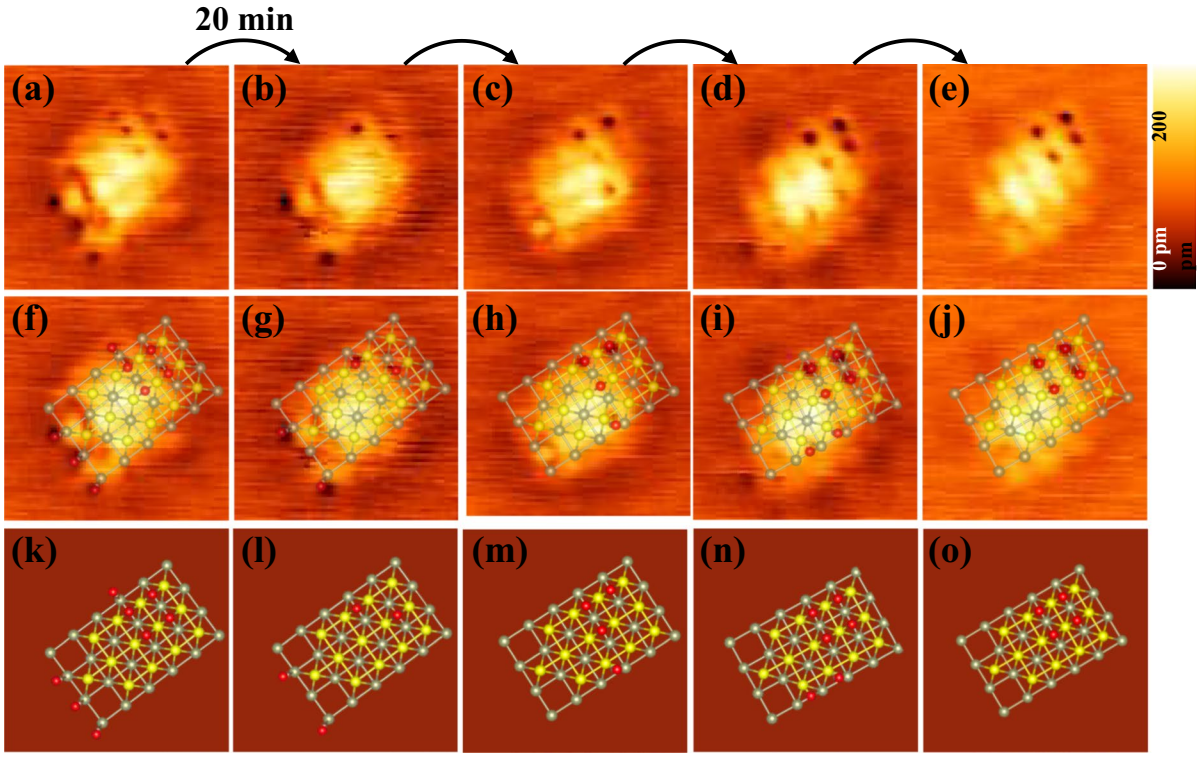

Fig. 5 **(a-e)** Consecutive scanning topographic AFM images of CO molecules on $Pd/Al_2O_3/NiAl$ surface at RT with recording every 20 min after 90 min of CO adsorption (1×10^{-6}torr). **(f-j)** Schematic models of CO adsorption on two layers of Pd NC. **(k-o)** AFM images with models. Red ball: CO; gray ball: Pd atoms in the first layer; yellow ball: Pd atoms in the second layer. Imaging parameters: constant-Δf mode, f_0 = 1.12 MHz, Q = 3304, and size: 4×4 nm^2

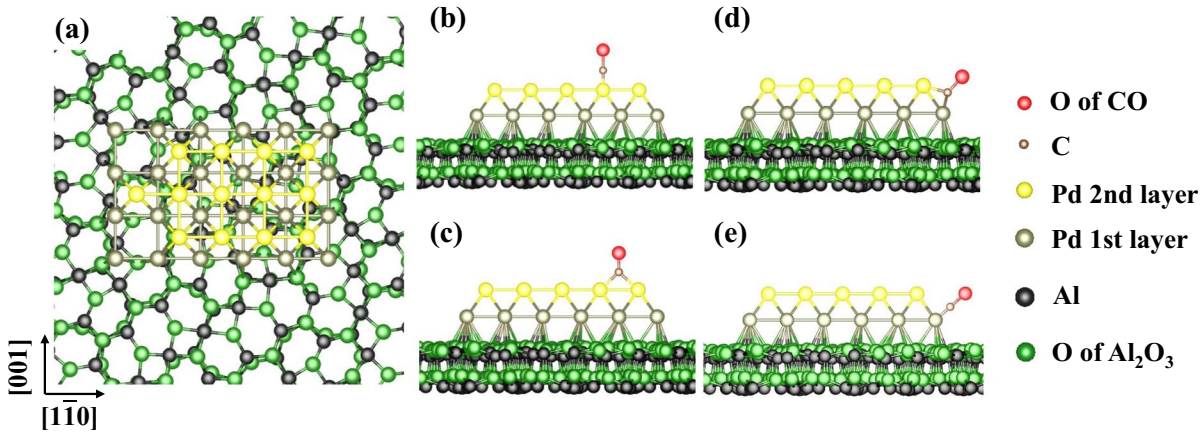

Fig. 6 Model of Pd NC on Al_2O_3 surface. **a** Corresponding schematic model of top view of Pd NPs on Al_2O_3 surface. Side views of CO molecule on top site **(b)**, bridge site **(c)**, step_111 site **(d)**, and step_110 site **(e)**

Table 1 Calculated adsorption energy (E_a) of CO molecule adsorbed at different sites

Site	Top site	Bridge site	Step_111 site	Step_110 site
E_a	-2.95eV	-3.68eV	-1.66eV	-1.07eV

Conclusions

We have investigated the adsorption behavior of CO molecules on Pd/Al_2O_3/NiAl(110) with atomic resolution by NC-AFM/KPFM at RT. We found that CO molecules are preferentially adsorbed on the Pd NC on line defects. Furthermore, from the CPD result, we found that the CO on the Pd NC is negatively charged. Combing experimental results with the DFT calculations, we found the most stable adsorption CO molecule is the bridge site, followed by the top site. And the most unstable adsorbed site was step_110. This result reveals that the electronic and geometric properties of Pd NCs and CO molecules are expected to provide insight into the mechanism of Pd-based heterogeneous catalysis.

Acknowledgments This work was supported by a Grant-in-Aid for Scientific Research from Japan Society for the Promotion of Science (JSPS) from the Ministry of Education, Culture, Sports, Science, and Technology of Japan (JP16H06327, JP16H06504 and JP17H01061). This work was also supported by the International Joint Research Promotion Program of Osaka University (J171013014, J171013007 and Ja19990011). This project was supported by Japan Society for the Promotion of Science (JSPS) and the National Natural Science Foundation of China (NSFC) (JSPS-NSFC (J191053055).

Compliance with ethical standards

Conflict of interest The authors declare no competing financial interest.

References

1. Schlögl R (2015) Heterogeneous catalysis. Angew Chem Int Ed 54(11):3465–3520
2. Rothenberg G (2017) Catalysis: concepts and green applications. John Wiley & Sons
3. Kunz L, Maier L, Tischer S, Deutschmann O (2012) Modeling the rate of heterogeneous reactions. ChemInform 43(36). https://doi.org/10.1002/chin.201236260
4. Klaewkla R, Arend M, Hoelderich WF (2011) A review of mass transfer controlling the reaction rate in heterogeneous catalytic systems, vol 5. INTECH Open Access Publisher, Rijeka
5. Lin X, Nilius N, Sterrer M, Koskinen P, Häkkinen H, Freund HJ (2010) Characterizing low-coordinated atoms at the periphery of MgO-supported Au islands using scanning tunneling microscopy and electronic structure calculations. Phys Rev B 81(15):153406
6. Gotterbarm K, Späth F, Bauer U, Bronnbauer C, Steinrück HP, Papp C (2015) Reactivity of graphene-supported Pt nanocluster arrays. ACS Catal 5(4):2397–2403
7. Yoon B, Hakkinen H, Landman U, Worz AS, Antonietti JM, Abbet et al (2005) Charging effects on bonding and catalyzed oxidation of CO on Au8 clusters on MgO. Science 307(5708):403–407
8. Beniya A, Higashi S, Ohba N, Jinnouchi R, Hirata H, Watanabe Y (2020) CO oxidation activity of non-reducible oxide-supported mass-selected few-atom Pt single-clusters. Nat Commun 11(1):1–10
9. Reşitoğlu İA, Altinişik K, Keskin A (2015) The pollutant emissions from diesel-engine vehicles and exhaust after treatment systems. Clean Technol Environ Policy 17(1):15–27
10. Van Vaerenbergh B, Lauwaert J, Vermeir P, Thybaut JW, De Clercq J (2020) Towards high-performance heterogeneous palladium nanoparticle catalysts for sustainable liquid-phase reactions. React Chem Eng 5(9):1556–1618
11. Kunz S, Schweinberger FF, Habibpour V, Röttgen M, Harding C, Arenz M, Heiz U (2010) Temperature dependent CO oxidation mechanisms on size-selected clusters. J Phys Chem C 114(3):1651–1654
12. Mistry H, Reske R, Zeng Z, Zhao ZJ, Greeley J, Strasser P, Cuenya BR (2014) Exceptional size-dependent activity enhancement in the electroreduction of CO_2 over Au nanoparticles. J Am Chem Soc 136(47):16473–16476
13. Gruene P, Fielicke A, Meijer G, Rayner DM (2008) The adsorption of CO on group 10 (Ni, Pd, Pt) transition-metal clusters. Phys Chem Chem Phys 10(40):6144–6149
14. Jakub Z, Hulva J, Ryan PT, Duncan DA, Payne DJ, Bliem R, Parkinson GS (2020) Adsorbate-induced structural evolution changes the mechanism of CO oxidation on a Rh/Fe_3O_4(001) model catalyst. Nanoscale 12(10):5866–5875
15. Bartels L, Meyer G, Rieder KH (1997) Basic steps involved in the lateral manipulation of single CO molecules and rows of CO molecules. Chem Phys Lett 273(5–6):371–375
16. Ternes M, Lutz CP, Hirjibehedin CF, Giessibl FJ, Heinrich AJ (2008) The force needed to move an atom on a surface. Science 319(5866):1066–1069
17. Sun Z, Boneschanscher MP, Swart I, Vanmaekelbergh D, Liljeroth P (2011) Quantitative atomic force microscopy with carbon monoxide terminated tips. Phys Rev Lett 106(4):046104
18. Schwarz A, Köhler A, Grenz J, Wiesendanger R (2014) Detecting the dipole moment of a single carbon monoxide molecule. Appl Phys Lett 105(1):011606
19. Huber F, Berwanger J, Polesya S, Mankovsky S, Ebert H, Giessibl FJ (2019) Chemical bond formation showing a transition from physisorption to chemisorption. Science 366(6462):235–238
20. Gameel KM, Sharafeldin IM, Abourayya AU, Biby AH, Allam NK (2018) Unveiling CO adsorption on Cu

surfaces: new insights from molecular orbital principles. Phys Chem Chem Phys 20(40):25892–25900
21. Parkinson GS, Novotny Z, Argentero G, Schmid M, Pavelec J, Kosak R, Diebold U (2013) Carbon monoxide-induced adatom sintering in a Pd–Fe_3O_4 model catalyst. Nat Mater 12(8):724–728
22. Berwanger J, Polesya S, Mankovsky S, Ebert H, Giessibl FJ (2020) Atomically resolved chemical reactivity of small Fe clusters. Phys Rev Lett 124(9):096001
23. Kou L, Ma Z, Li YJ, Naitoh Y, Komiyama M, Sugawara Y (2015) Surface potential imaging with atomic resolution by frequency-modulation Kelvin probe force microscopy without bias voltage feedback. Nanotechnology 26(19):195701
24. Arima E, Wen H, Naitoh Y, Li YJ, Sugawara Y (2016) Development of low temperature atomic force microscopy with an optical beam deflection system capable of simultaneously detecting the lateral and vertical forces. Rev Sci Instrum 87(9):093113
25. Kou L, Li YJ, Kamijyo T, Naitoh Y, Sugawara Y (2016) Investigation of the surface potential of TiO_2 (110) by frequency-modulation Kelvin probe force microscopy. Nanotechnology 27(50):505704
26. Zhang Q, Li YJ, Wen HF, Adachi Y, Miyazaki M, Sugawara Y, Štich I (2018) Measurement and Manipulation of the Charge State of an Adsorbed Oxygen Adatom on the Rutile TiO_2(110)-1×1 Surface by nc-AFM and KPFM. J Am Chem Soc 140:15668–15674
27. Miyazaki M, Wen HF, Zhang Q, Adachi Y, Brndiar J, Štich I, Sugawara Y (2019) Imaging the surface potential at the steps on the rutile TiO_2 (110) surface by Kelvin probe force microscopy. Beilstein J Nanotechnol 10:1228–1236
28. Zhang Q, Brndiar J, Konôpka M, Wen HF, Adachi Y, Miyazaki M, Li YJ (2021) Unraveling the Charge States of Au Nanoclusters on an Oxygen-Rich Rutile TiO_2 (110) Surface and Their Triboelectrification Overturn by nc-AFM and KPFM. J Phys Chem C 125(50):27607–27614
29. Perdew JP, Burke K, Ernzerhof M (1996) Generalized gradient approximation made simple. Phys Rev Lett 77(18):3865
30. Giannozzi P, Baroni S, Bonini N, Calandra M, Car R, Cavazzoni C, Wentzcovitch RM (2009) QUANTUM ESPRESSO: a modular and open-source software project for quantum simulations of materials. J Phys Condens Matter 21(39):395502
31. Gao Y, Zhang LM, Kong CC, Yang ZM, Chen YM (2016) NO adsorption and dissociation on palladium clusters: the importance of charged state and metal doping. Chem Phys Lett 658:7–11
32. Stierle A, Renner F, Streitel R, Dosch H, Drube W, Cowie BC (2004) X-ray diffraction study of the ultrathin Al2O3 layer on NiAl (110). Science 303(5664):1652–1656
33. Schmid M, Shishkin M, Kresse G, Napetschnig E, Varga P, Kulawik M, Freund HJ (2006) Oxygen-deficient line defects in an ultrathin aluminum oxide film. Phys Rev Lett 97(4):046101
34. Deguchi T, Iwamoto M (2013) Catalytic properties of surface sites on Pd clusters for direct H_2O_2 synthesis from H2 and O2: a DFT study. J Phys Chem C 117(36):18540–18548
35. Xia M, Ding W, Xiong K, Li L, Qi X, Chen S, Wei Z (2013) Anchoring effect of exfoliated-montmorillonite-supported Pd catalyst for the oxygen reduction reaction. J Phys Chem C 117(20):10581–10588
36. Caciuc V, Hölscher H, Blügel S, Fuchs H (2006) First-principles study of the atomic-scale structure of clean silicon tips in dynamic force microscopy. Phys Rev B 74(16):165318
37. Finazzi E, Di Valentin C, Selloni A, Pacchioni G (2007) First principles study of nitrogen doping at the anatase TiO_2 (101) surface. J Phys Chem C 111(26):9275–9282
38. Kresse G, Schmid M, Napetschnig E, Shishkin M, Kohler L, Varga P (2005) Structure of the ultrathin aluminum oxide film on NiAl (110). Science 308(5727):1440–1442
39. Li YJ, Brndiar J, Naitoh Y, Sugawara Y, Štich I (2015) Atomic force microscopy identification of Al-sites on ultrathin aluminum oxide film on NiAl (110). Nanotechnology 26(50):505704
40. Zou S, Yokoyama H, Sugawara Y, Li YJ (2020) Size dependence of charge state of Pd nanoparticles on the Al_2O_3/NiAl(110) surface by Kelvin probe force microscopy. J Phys Chem C 124(39):21641–21645
41. Sung SS, Hoffmann R (1985) How carbon monoxide bonds to metal surfaces. J Am Chem Soc 107(3):578–584
42. Sader JE, Jarvis SP (2004) Accurate formulas for interaction force and energy in frequency modulation force spectroscopy. Appl Phys Lett 84(10):1801–1803